Chapter 3

BUBBLES AS OCEANOGRAPHIC OBJECTS

All physical bubble-related processes, theoretically considered in Chapter 2, find their place in the real ocean in a complex interplay. Once formed, the bubbles in the ocean do experience growth or collapse under gas diffusion, surface tension or pressure changes, an influence of the heat transfer on their walls, rise due to buoyancy force and so on. However, all these are modified by the complex motion of the surrounding water and the sea water composition, not to mention the atmosphere's influence, in such a subtle way that often it is impossible to distinguish which environmental parameter causes a particular behavior of the bubble.

3.1 Significance

In oceanography both, the individual bubbles and bubble clouds play an important role. As individual objects within a stable background population, bubbles rise and

burst on the sea surface and produce marine aerosol. Eriksson (1959) estimated that the sea through bubble bursting delivers salt particles in the atmosphere with a rate in the order of 1000 million tons per year. The loading of the marine environment with salt particles (Woodcock, 1972; Blanchard, 1985) makes it highly corrosive and has consequences on the cloud formation (Blanchard and Syzdek, 1972; Latham and Smith, 1990) . Bubble bursting enriches the atmosphere with bacteria (Blanchard, 1983), heavy metals (Duce and Hoffman, 1976), and organic mass (Hoffman and Duce, 1977) as well. Through sea spray evaporation, bubbles are involved in the exchange of heat and moisture between the ocean and atmosphere (Andreas et al., 1995) . Bubbles enhance the gas transfer of climate relevant gases, such as O_2 and CO_2, across the air-sea interface (Merlivat and Memery, 1983; Leifer et al., 1995; Geißler and Jähne, 1995) . Bubble volume oscillations in the turbulent field beneath the breaking wave contribute to the ocean ambient noise (Prosperetti, 1988; Medwin and Beaky, 1989) .

Apart from the population of individual bubbles, the bubbles entrained *en mass*, bubble clouds, are important. Similarly to the clouds of liquid drops in the atmosphere, the clouds of bubbles under the water surface can be helpful to elucidate the dynamics of mixing of the upper ocean layer (Thorpe, 1992) . The temporal and spatial evolution of the cloud shape and its penetration depth can be used to clarify the processes of convection, turbulence, and diffusion. The surface bubble layer alters the oceanic background sound level and sound-speed structure (Farmer and Valge, 1989) . The sound speed in water can be reduced by an order of magnitude in the presence of void fractions as low as 1% (Lamarre

and Melville, 1991) . The initial bubble population, immediately after breaking, is very dense, especially at high winds (> 12 m s^{-1}) . It features a wide range of bubble sizes and the prevalence of large bubbles (0.5 - 8 mm) is considerable. Keeling (1993) had concluded that bubbles greater than 0.5 mm in radius contribute significantly to bubble-induced air-sea gas exchange. However, these traits are short-lived: large bubbles, being more buoyant, rise to the surface quickly, altering the initial bubble distribution. The models of bubble mediated gas transfer depend on reliable estimates of exactly this initial, and not the later equilibrium, bubble size spectra (Keeling, 1993; Melville et al., 1995) . For all these processes measuring and quantifying the void fraction of the bubble cloud instead of individual bubbles distribution is useful.

The bubble clouds beneath the water and the white bubbly patches floating on the sea surface represent the two types foam (§2.7.3) that comprise the whitecaps. Both types change the ocean albedo significantly as the reflective characteristics of the water with and without foam are very different (Koepke, 1986; Frouin et al., 1996) .

3.2 Formation

Bubbles exist in the ocean in two populations. Bubbles in equilibrium with sizes less than 0.4 mm form a layer of background persistent population about 1 m thick (Monahan and Lu, 1990; Wu, 1994) . This bubbly layer is constantly overlapped by intermittent and relatively shortly living bubble clouds, representing the transient bubble population. The background population comes from the decay of whitecaps and stabilized

microbubbles, and from secondary sources such as raindrops, snowflakes, supersaturation of seawater by temperature changes, biological activity, falling of a continental aerosol on the water, and sediment outgasing (Blanchard and Woodcock, 1957; Johnson, 1986) .

Blanchard and Woodcock (1957) observed that when a snowflake melts 50 to several hundred bubbles were released. The raindrops produce bubbles directly in the moment of their impact on the sea surface, and indirectly through the drops splashed during the impact or drops that float shortly on the surface. Though producing significant number of bubbles, these two sources require precipitation, hence they are important only locally and temporarily. The dissolved air content in the oceanic surface layer is usually at or near saturation and varies with the seasons. As the solubility of the air is an inverse function of the temperature, it follows that at saturation values a maximum would appear near the end of the winter when the water is coldest and a minimum at the end of summer when the water is warmest. In spring supersaturation may happen if for a short time span the water is intensely heated by warm overlaying air. If the supersaturation by heating keeps ahead of the gas loss by diffusion and there are sufficient nuclei, bubbles may form (recall the influence of the gas in heterogeneous cavitation, §2.2.1) . But the rapid and large temperature changes required for the supersaturation are not common in the sea and thus supersaturation is not likely mechanism. Falling of a continental aerosol on the sea produces insignificant amount of bubbles. Biological processes are the major source of the background population which, however, is mostly confined near the shore. So, in absence of precipitation and in wind speeds exceeding about 3 m s^{-1} wave breaking manifested as whitecaps is the major source

for bubble production in the ocean. The whitecaps indicate the formation of the transient bubble population and the consequent fast decay through rising of the largest and dissolving of the smallest bubbles. But long after the whitecap ceases to be visible significant concentrations of smaller bubbles are still present in the water. What happens is that plumes of bubbles with some intermediate size penetrates deeply, surface active materials stabilize them and eventually they join the equilibrium population.

The dynamics of the breaking process, and in particular the dense two-phase (liquid/gas) mixture formed during and immediately after collapse, is a subject still under investigation. Wave breaking results from a combination of nonlinear hydrodynamic and aerodynamic processes that are only qualitatively understood. The common idea in the models for wave breaking is that the process occurs when some random variable exceeds a critical value. There are four commonly accepted criteria for surface wave instability that eventually can lead to wave breaking (Walker, 1994): 1) the fluid velocity at the wave crest exceeds the phase velocity of the wave $U \geq c$; 2) the fluid vertical acceleration at the crest exceeds the gravitational restoring force, $|a_z| \geq |g|$; 3) the free surface slope becomes vertical and overturns; 4) the pressure at the free surface exceeds that allowed by Bernoulli' equation, i.e. Kelvin-Helmholtz instabilities occur. There are two basic types of breaking waves: spilling and plunging. The observation and quantification of the fast process of breaking give insights for the transfer of momentum from waves to currents, the wave energy dissipation, and the turbulent mixing in the water column (Longuet-Higgins and Turner, 1974; Rapp and Melville, 1990) .

Observations of the air entraining and formation of bubbles are usually made with a photographic technique. A few descriptions of the bubble entrainment can be found in the literature. Koga (1982) photographed the process of bubble cluster formation and spreading in a laboratory study under 16 m s^{-1} wind. He pictured a transportation of the bubbles under the leading slope of the wave by an ordered downward water flow formed on the leading wave slope near the crest. Later, turbulence and different bubble rising velocities redistribute the initial bubble cluster into isolated bubbles aligned under the windward wave slope. From the bubbles' movement he estimated the flow velocity (0.4 - 1.2 m s^{-1}) . Rapp and Melville (1990) also photographed different stages of a mechanically formed spilling and plunging breakers and observed the formation and evolution of a bubble cloud. Their photographs depict the wave steepening and asymmetry in the moment just before breaking. For spilling breaker the free surface breaks up close to the crest and entrains air which forms bubbles. For plunging breaker a well defined jet is formed which curls, encloses a pocket of air and impacts the forward wave face causing a secondary jet to appear. The entrained air spreads forward and in depth. Longuet-Higgins (1988) summarized the main traits of the whole process for a plunging breaking wave on the basis of Melville and Rapp (1985) work: 1) the water jet strikes the forward wave face and partly rebounds producing droplets; when droplets fall onto the water they form bubbles; 2) the part of the jet which penetrates the water surface entrains with it a large quantity of air, which immediately breaks into bubbles; 3) additional amount of air, entrapped in a "tube" from the curled crest, is forced downward into the water to form a cloud of bubbles. Lammare (1993) captured with an underwater video camera the initial instabilities and peculiar finger-like structures which led the smooth

air "tube" to break into a complex turbulent bubbly mixture. The process of air entrainment is similar for the spilling breaking but on a diminished scale (Thorpe, 1992) . Duncan (1981) made a systematic experimental study of breaking waves and quantified the air-entraining turbulent region, riding on the wave's forward slope. Steady breakers were produced by towing a hydrofoil at different speeds, depth and angle of attack in a tank. Photographs of the surface profiles and dyed turbulent wake of the breakers were taken. The parameters chosen to quantify the turbulent aerated zone (the breaking region) are length, area, thickness, inclination. These are scaled with the wave characteristics. The measurements show that the breaking region produces a shearing force along the wave slope which produces a turbulent wake.

Models on the breaking and air entrainment processes have been tried, but usually they stop at the moment of the jet impact on the water surface (Rapp and Melville, 1990) . The reason is that the turbulent breaker can not be analyzed by the method of potential flow which is usually employed by the numerical models to follow the wave evolution up to the point of breaking (Longuet-Higgins and Turner, 1974) . The only dynamical model (Longuet-Higgins and Turner, 1974) of aeration (whitecap) following the breaking is for a spilling breaker. Several features of the spilling breaker can be described when the whitecap is considered as a turbulent plume, running down the forward wave slope and entraining the laminar fluid from below it. At the beginning, the spilling waves break gently at the crest and trap enough air bubbles for the resulting air-water mixture to be significantly lighter than the water below it and to inhibit mixing with the wave. The density difference between the water wave and the plume is the driving force causing the whitecap

to ride on the top of the sloping water surface. Hence, the basic assumption in the model is that the plume can be regarded as a distinct turbulent flow driven down the wave slope by the gravity, very much like a gravity flow moving down the continental slope. Later on, as the flow continues, turbulence entrains more water from the laminar wave below, which, in turn, further incorporates air, especially near the front of the whitecap, thus maintaining the density difference. The rate at which water is entrained in the plume depends on the velocity difference between the whitecap and the wave, on the density difference of the water and the air-water mixture, and on some local length scale, which is typically chosen to be the mean thickness of the plume. Much less information is provided from the model on the entrainment of air from above. Consensus of laboratory studies is that the process of aeration can be explained in two ways. One way air can be incorporated in the whitecap is the over-running of a layer of air by the advancing front, usually observed in hydraulic jumps. Another way for air entrainment is the "self-aeration" which occurs when the turbulent boundary layer of the bottom reaches the free surface and is energetic to overcome the surface tension energy, so to allow eddies to project out of the surface and trap bubbles. In the early stages of all breakers, over-running at the front is usually the only way in which air is trapped, but at later stages whitecaps sustain themselves by self-aeration (Longuet-Higgins and Turner, 1974) . The model obtains a solution for the spilling breaker under the assumptions that the flow is steady in time (i.e., it does not grow), and that the slope and the density difference are constant. The theory shows that the steady motion is sustained when the density difference is greater than 8%. The solution is in term of the distance from the point of measurement and the wave crest s: the thickness of the whitecap is proportional to s; the velocity is

proportional to $s^{1/2}$. The solution for the steady case is used to describe the unsteady case (the flow increases in length with time) using so called "starting plume" model. According this model, the whitecap is accelerated uniformly down the wave slope. At the front of the plume extra water accumulation forms a vortex-like circulation zone where greater amount of air and water penetrates the wave surface. The comparison of the model with laboratory observations revealed a general increase in the plume parameters with time, and also marked intermittency. From energy balance it is found that the length of the whitecap should be a fraction of the wave height, about one half. As in shallow water the wave height tends constantly to diminish, it follows that a steady state cannot normally be achieved, and therefore the whitecap can exist only intermittently. The most recent model has been proposed by Cointe and Tulin (1994) . They actually present a theory of the quasi-steady breakers, created above a submerged hydrofoil and studied experimentally by Duncan (1981). A breaker created by a hydrofoil is an example of a flow in which the resistance of a submerged body manifests itself in an eddy located away from the body, i.e., on the free surface. The model explains the conditions for the inceptions of this separation and predicts the breaking configuration. Similarly to Longuet-Higgins and Turner (1974), the physical idea is that the breaker consists of an stagnant eddy riding on the wave slope, and sustained by the turbulent stress acting in the shear zone between the eddy and the underlying water flow. The parameter under consideration is the degree of aeration. This theory cannot be applied to non-steady breaking waves in the sea. Non-steady breaker theory is required for the open ocean conditions.

Another two mechanisms for air injection are the breaking of short waves riding on the crest of longer waves and the generation of capillary waves on the forward faces of short gravity waves (Thorpe, 1992) . Laboratory study on the height and period of breaking gravity waves (Xu et al., 1986) provide an evidence for the coexistence of two distinct populations from breaking, perhaps reflecting these two different mechanisms.

3.3 Oceanic Processes Involving Bubbles

The main processes in which the bubbles and bubble clouds are involved are: 1) the mixing in the upper ocean layer by the breaking waves induced turbulence; 2) gas exchange between the ocean and the atmosphere; 3) marine aerosol production by bursting of bubbles on the sea surface; 4) production of ambient noise in the ocean. Two of these processes and the effect of sea water composition on bubble production and distribution are considered in the next paragraphs.

3.3.1 Mixing in the Upper Layer

The oceanic bubbles within the equilibrium population, being less than 0.4 mm in size, are spherical and hence in quiescent water would rise to the surface along a linear path (refer to §2.2.3) . As the initial dense population immediately after breaking consist of a wide range of sizes, the bubble shapes vary from spherical to ellipsoidal. Most of the large bubbles (> 400 μm) within the clouds are ellipsoids and, being buoyant, surface quickly winding on a helical path.

The bubble rise velocity, V_r, is driven by the pressure p in the water at depth D, $p = p_0 + g\rho D$ (p_0 is the atmospheric pressure), and is affected by the downward velocity component, U, of the surrounding water (Thorpe, 1982): $dp/dt = g\rho(U-V_r)$. If $V_r > U$, the bubbles will not be carried downward by the water, but will rise. The rise velocity is additionally affected by the state of the bubbles. Surface active material is rapidly adsorbed (details in §3.3.2) by the small bubbles and then they behave dynamically as rigid bodies. In contrast to these *dirty* bubbles, as they are called in oceanography, the newly entrained *clean* bubbles do not carry organic film at the beginning. Clean bubbles of radii less than about 100 μm however become dirty in a few tens of seconds, which is very short time compared to their lifetime, hence the size is stabilized by the film, and therefore these can be expected to behave as rigid particles always. On the large bubbles the organic film is not uniformly distributed. The shear flow of the water past the bubble compresses the film toward the lower side of the bubble, thus they are expected to behave as deformable particles. The drag is increased and the bubble moves more and more slowly. The bubble size for which $V_r = U$ can be considered as a critical radius and all bubbles with size less than the critical will be pushed deep in the water. This critical size would be different for dirty and clean bubbles.

It seems that the vertical distribution of the bubbles is governed by both, the buoyancy and the turbulence, while the horizontal dispersion is mostly associated with the turbulence near the surface and the Langmuir circulation. The bubbles are carried downward by the turbulence in the upper ocean layer. It is observed that the bubbles reaching only a meter beneath the surface are very small. Also, according field measurements made by Thorpe and Hall (1983), they persist typically for periods of 5 - 10 minutes. Therefore, the

relevant turbulent motion is that which is effective in producing diffusion on these scales: time scale perhaps from a second up to an hour, and space scale from the Kolmogorov scale (typically of the order of 1 cm) to a depth about the mixed layer thickness and in horizontal plane in order of the length of largest waves (Thorpe, 1992) . There are laboratory and field experiments which provide evidence that the turbulence derived directly from the breaking waves may be limited to a relatively narrow zone beneath the sea surface. By photographing a dye patch Rapp and Melville (1990) tracked the turbulent mixing in the water column. They found that the maximum depth (two to three wave heights) of the dye cloud grew with time for one to two wave periods following a $t^{1/4}$ power law. Thorpe (1992) describes an experiment with a sonar from a submarine which showed a distinct correspondence between the enhanced values of turbulent dissipation and the acoustically registered bubble clouds. The turbulent dissipation values were largest close to the surface at locations associated with bubbles. Kitaigorodski et al. (1983) suggest that the effect of breaking waves dominates and enhances the turbulence to a depth about ten times the root-mean-square wave amplitude, which is in the range 0.04L to 0.16L of the wave length L (Thorpe, 1992) . This is consistent with the bubble cloud penetration depth observed by Thorpe (1992) . Therefore, the near-surface turbulence is most probably related to and enhanced by the bubble clouds.

However, many experiments also show that the turbulent dissipation rate at depths beyond this near-surface turbulent layer are exceptionally high. In addition, the turbulent dissipation below about 10 m depth was not relevant to the bubble clouds positions any more. This suggests that some other process of turbulent dissipation take place and there is an evidence that this could be the Langmuir circulation. Most of the experiments

confidently suggest that the Langmuir circulation may be important for the mixing up to the middle of the mixed layer, however the results for mixing down to 40-60 m depths are not conclusive yet. But there is little doubt about the Langmuir circulation effect on the ordering of the dispersed floating and buoyant bubbles. Indeed, Thorpe and Hall (1983) reported the observation of bubble bands, eventually consisting of bubbles produced by breaking waves and carried down by the convergent flow of the Langmuir circulation.

3.3.2 Effects of the Sea Water Composition

The many types of substances dissolved in the ocean can be divided into five chemical groups: major constituents, nutrients, gases, trace elements, and organic compounds. The salinity of the water is acquired mainly from two ionic components: sodium (Na^+) and chloride (Cl^-) (Pinet, 1992) . The organic compounds include complex organic molecules like lipids (fats), proteins, carbohydrates etc. Such organic and inorganic chemicals can establish a surface active film on the open ocean surface and on the interfaces of the rising bubbles. The film on the open ocean surface affects the water motion by two factors: the surface tension and surface dilatational elasticity (Scott, 1986) . For example, the velocity of the ripples on the water is strongly influenced by the surface tension, but the elasticity damps them. For gravity waves the surface tension loses its importance, but the elasticity is still the determining factor for the wave damping. The stabilizing effect exerted on the surface by the film dilatational elasticity leads to marked reduction of the energy input to the waves and as a result retardation or even prevention of the breaking processes may occur.

This influences the rate of bubble production indirectly. In addition, through these films the water composition influences the formation, lifetime and the dynamics of the bubbles which is ultimately expressed in the difference of the bubble population and whitecap signature in salt and fresh waters.

The surface activity of the organic components reduces the surface tension of sea water compared to that of fresh water, so the air entrained breaks readily into more and smaller bubbles. In addition, the organic mater, attached to the bubble surface during its rising through the water column, stabilizes it and delays the bubble dissolution (Blanchard, 1983) . The presence of inorganic salt slightly increases the surface tension of the sea water (§2.7.2) but this effect is easily suppressed by minute organic materials so that ultimately it does not alter the bubble behavior. The main effect of the inorganic salts is on the bubble coalescence. The ionic nature of the saline water, arising from the presence of inorganic salt, inhibits the coalescence between bubbles as repulsive forces come into play when they approach each other (Scott, 1975) . This, together with the stabilizing mechanisms of the organic film (§2.7.2), helps bubbles to stay smaller, to be more numerous and to pack more densely for a given volume of entrained air. Overall the consequences are: 1) the surface area available for gas transfer from and to the bubbles is larger; 2) bubbles, being smaller, rise to the surface more slowly; 3) small bubbles will be carried deeper into the water. All these three effects lead to more efficient mixing of atmospheric gases introduced into the water column. Also, the scavenging of organic and/or any other surface active materials to the surface and their consequent expelling into the atmosphere through bubble bursting is enhanced.

On the sea surface the organic films stabilize the bubble lifetime. The longevity of floating air bubbles on the air-water surface has been frequently investigated. Garrett (1967) found in the absence of a surface film that the lifetime of an air bubble was determined by the surface-active material adsorbed during its rise. The presence of compressed monomolecular layer at the sea surface reduced the bubble stability and acted as an antifoaming agent. Struthwolf and Blanchard (1984) measured the surface residence time of air bubbles with diameters from 50 to 400 μm in distilled and sea water. In distilled water all bubbles > 200 μm lived less than 0.05 s, but the smaller bubbles persisted for several seconds, which is in accord with the interpretation in §2.7.1 that even distilled water has some impurity which can cover the smallest bubbles with a film and stabilize them. In sea water they found opposite trends: the small bubbles broke almost immediately (< 0.01 s) while the larger bubbles resided for 0.3 s. The stable residence of air bubbles on the water surface under decreased relative humidity or increased speed of air was explained successfully by the stabilizing action of the Gibbs and Marangoni effects (Burger and Blanchard, 1983) . Zheng et al. (1983) documented in a laboratory study the statistical characteristics of the bubble surface lifetime on sea water samples. The distribution of the bubble lifetime times was a Rayleigh type and the mean values depended on the bubble size. The surface foam in sea was systematically studied by Abe (1962) . He introduced *foaming factor* which is useful for indicating the foaming ability of the water. The stability and decay of a thick foam layer at different salinities of the water was investigated by Peltzer and Griffin (1987-88) . The results showed that varying the salt content of a clean water between 0 and 16 ppt significantly influenced the foaming ability and the stability of the layer. For salinities between 20 and 36

ppt there were no appreciable changes. The behavior of real sea water closely followed that of the simulated sea water.

3.3.3 Bubble Mediated Gas Exchange

The flux of gases to and from a water body can be estimated as the product of the air-water concentration difference, ΔC, of a gas and its transfer velocity, k (Liss, 1983). Because of the difficulties associated with direct oceanic measurements of k, it is often calculated from parametrizations derived empirically from wind speed. The exchange of gases between the ocean and atmosphere is influenced from geochemical, biological and physical processes. Molecular and turbulent diffusion are the main physical processes for gas transfer. As the diffusion is strongly influenced by environmental conditions, the affect of wind, waves, and bubbles are usually considered. The laboratory experiments show a clear increase in transfer velocity with an increase of the wind speed. The trend is mild up to a wind speed of about 8 m s^{-1}, there is a jump in the transfer velocity by about a factor of 5 thereafter. A marked increase appears with the onset of waves, most probably because ripples augment the area available for gas exchange. However, it was estimated (Hasse and Liss, 1980) that the increase in area due to capillaries is at most 50%, so the effect is probably not of great quantitative importance. Nevertheless, the capillary waves can indicate a change in the nature of gas-transfer process. The abrupt change in transfer velocity slope at 8 m s^{-1} wind was then attributed to appearance of breaking waves and bubbles. It was suggested (Asher et al., 1996) that the transfer velocity can be partitioned into one component due to the near-surface

turbulence generated by currents and nonbreaking waves (k_m), one due to turbulence generated by breaking waves (k_t), and one due to bubble-mediated transfer (k_b) . For gas evasion with $\Delta C << 0$, k can be written in terms of the fractional area of whitecap coverage, W, as

$$k = [k_m + W(k_t - k_m)] + Wk_b.$$

Laboratory results demonstrated (Asher et al., 1996) that bubble clouds enhance gas transfer by directly transporting gas and by creating turbulence. The gas flux due to bubbles was modeled by Merlivat and Memery (1983), Woolf and Thorpe (1991), and Keeling (1993) . Contrary to gas transfer across the air-water interface, where the transfer is solely controlled by surface turbulence and the molecular diffusion coefficient of the gas, the exchange through bubbles is also a function of the solubility of the gas, bubble size and bubble penetration depth (Keeling, 1993; Wanninkhof et al., 1995) . If the bubble exchange is important, the transfer velocity should increase roughly in proportion to the area covered with whitecaps. While the exchange across the ocean-atmosphere interface drives the concentration of the dissolved gases toward equilibrium with the atmosphere, bubble exchange drives the seawater toward a slight supersaturation because the air in the bubbles is compressed by the surface tension and hydrostatic pressure.

3.4 Main Characteristics

The main characteristic of the bubbles from oceanographic point of view is the bubble size distribution defined as the number of bubbles per unit volume and per radius band.

Usually the dependence of this distribution on depth and wind speed is sought. The effect of temperature and salinity on the size distribution is also of interest.

The mixture of water and air bubbles, bubble clouds, can be characterized by the void fraction α defined as the volume occupied by the bubbles in a unit volume of the mixture. If N(r) is the number of bubbles per unit volume per radius increment dr, and each bubble has a volume $V_b(r)$, it is evident that the void fraction of the bubble cloud is

$$\alpha = \int_r N(r)V_b(r)dr = \int_r \frac{4}{3}\pi N(r)r^3 dr$$

This equation suggests that by knowing the bubble size population the void fraction can be easily obtained. However, as the bubble concentration increases with increasing wind speed, most of the techniques for bubble size measurements reach their limit. Their ability to distinguish the individual bubbles and to measure precisely a wide range of bubble sizes diminishes. Therefore, it is essential to find a reliable way to measure the void fraction instead of the population of individual bubbles.

3.5 The Pioneers in Oceanographic Bubble Measurements

The significance of bubbles in different oceanographic processes inspired many field and laboratory efforts to detail the knowledge on their effects in the near-surface ocean. First, Blanchard and Woodcock (1957) published all they had learned about how bubbles are produced in the sea, together with some measurements of bubbles size spectra beneath

breaking waves. They used a small box (9 x 6 x 2 cm) with one transparent side, the opposite side being removable, to take a sample of the cloudy sea water a few seconds after a breaking wave had passed in a coastal zone. They found that at a depth of 0.1 m and a water temperature of 21°C the concentration of bubbles was of the order of 10^8 m^{-3} and their diameters were in the range 100-500 μm with peak around 100 μm. Medwin (1970) introduced the acoustic method in bubble measurements. Bubble concentration of 10^3 m^{-3} in radius range 18 - 180 μm in coastal water at depths up to 15 m was measured. Kolovayev (1976) used bubble trap to measure bubbles in open ocean at depths of 1.5 - 8 m and water temperature of 16-17 °C under wind speeds of 6 - 13 m s^{-1}; he reported concentrations of order 10^4 - 10^3 m^{-3} in radius range 15 - 350 μm with peak around 60 - 70 μm. Johnson and Cooke (1979) employed a photographic method under wind velocity 8 - 13 m s^{-1} at depths 0.7, 1.5 and 4 m and water temperature of 2 °C; they found bubble density from $4.8x10^5$ to $1.6x10^4$ m^{-3} for radii 17 - 300 μm with peak around 50 μm. These results were reviewed by Wu (1981) to obtain depth and wind dependencies of bubble population and size distribution. The distributions obtained in these pioneering works are reproduced in Figure 3.1.

3.6 Principle Results of Bubble Studies

Although these pioneering and later measurements were made at different wind speeds, depths, meteorological conditions, and instrumental resolution, the accumulation of data (Koga, 1982; Crawford and Farmer, 1987; Walsh and Mulhearn, 1987; Baldy, 1988; Ling and Pao, 1988; Su et al., 1988; Medwin and Breitz, 1989; Hwang et al., 1990)

Figure 3.1 Bubble size spectra measured by: a) Blanchard and Woodcock (1957); b) Kolovayev (1976); c) Johnson and Cooke (1979); d) Medwin (1970) .

allowed a general description of bubble populations near sea surface (Wu, 1988a; 1992a) . Results of different investigations are summarized in Table 3.1.

Table 3.1(from Lamarre, 1993)

3.6.1 Bubble Size Distribution

Bubble size distribution can be empirically expressed by (Wu, 1992a):

$$p(d) = 6.25 \times 10^{-10}\, d^{4} \qquad d < 70\ \mu m$$

$$p(d) = 0.015 \qquad 70\ \mu m < d < 100\ \mu m$$

$$p(d) = 1.5 \times 10^{6}\, d^{-4} \qquad d > 100\ \mu m,$$

where p(d) is the frequency of occurrence of bubbles of diameter d. The frequency of occurrence p(d) is obtained by normalizing the bubble size spectra derived by Kolovayev and Johnson and Cooke with the total bubble population, result of summing up of all bubble counts (Wu, 1988a) . The expressions give the background bubble concentration, considered to be low but persistent over the entire sea surface layer. Beneath breaking waves bubble population is very high but only for a while (Blanchard, 1983) .

3.6.2 Shape of the Size Spectrum

The shape of the size spectrum, obtained at various conditions, is approximately invariant and peaked at a small plateau around 75 μm, Figure 3.2. (Actually, there is a debated about the presence of this peak; the issue is discussed in §4.4.) The dropoff on the large-diameter side varies from -2.5 to -6 for different experiments and this is associated mainly with the water temperature. The largest bubble observed is over 10 mm, but in very low concentration. Bubble size spectrum narrows slightly with depth. Only

smaller bubbles are carried down to 10 - 20 m depths by turbulence and Langmuir circulation. The size and concentration of the smallest bubble are uncertain not only because of technical restrictions to resolve such sizes but also because the small bubbles go into solution in less than a minute due to the surface curvature effects. (Some bubbles, stabilized by organic film, may not dissolve so quickly.) Bubbles smaller than 15 - 17 μm (Kolovayev, 1976; Johnson and Cooke, 1979) have not been observed.

Figure 3.2 Complete bubble spectrum (from Wu, 1992a) .

3.6.3 Wind and Depth Dependencies

Wind dependency of the bubble population N in m^{-3} is parameterized on the basis of data by the expression (Wu, 1992a)

$$N=57\ U_{10}^{\ 3.5}\ ,$$

$$N=2.9x10^{6}\ u_{*}^{\ 3}\ ,$$

where U_{10} in m s^{-1} is the wind velocity at 10-m elevation and u_* in m s^{-1} is the friction velocity. For wind less then 3 m s^{-1} this relation is not valid, because bubbles are not observed (Thorpe, 1982) .

Depth dependency of the bubble concentration shows an exponential decrease with depth z from surface value N_0 to N(z) (Wu, 1988a):

$$N(z)/N_0 = \exp(z/z_b),$$

where $z_b = 0.4$ $U_{10} < 7$ m s^{-1}

$z_b = 0.4 + 0.12(U_{10} - 7)$ $U_{10} > 7$ m s^{-1}.

The parameter z_b characterizes the vertical entrainment of bubbles. The particular wind value of 7 m s^{-1} is associated with the wind velocity at which the atmospheric surface layer becomes aerodynamically rough.

Whitecap coverage, the main source of bubble production among others suggested by Blanchard and Woodcock (1957), is estimated to be at most 3% of the sea

surface. It is strongly dependent on wind speed and empirical expression had been first proposed by Monahan and O'Muircheartaigh (1980)

$$W = 3.84 \times 10^{-6} U_{10}^{3.41},$$

and later, on the basis of previous analytical and experimental data, Wu (1988b) suggested

$$W = 1.7 U_{10}^{3.75}$$

where U_{10} is the wind speed at a 10-m elevation. In terms of friction velocity u_*, cm s^{-1},

$$W = 0.2 u_*^3 .$$

3.6.4 Additional Effects

Water temperature affects the inception of bubbles: low temperatures hinder the bubble production and their downward entrainment (Hwang et al., 1991) . For the experimental conditions in this laboratory study, there was a critical temperature, 11°C, below which bubbles were not generated. Obviously this laboratory result can not be applied directly to ocean conditions: Johnson and Cooke (1979) did measure bubbles in 2 - 3°C water temperature. However, the field observations proved that size spectra measured in cold water have a much narrower size range. The broadening of the bubble size spectra at higher temperatures is consistent with the conclusion that bubble production is enhanced in warm water. Also, the depth of bubble penetration in winter was documented to be approximately half the fall values, which suggests that downward entrainment was hampered.

The whitecaps in the sea are more persistent compared to these in fresh water (Monahan and Zietlow, 1969; Scott, 1975; Su and Cartmill, 1995) . Two effects, elucidated in §3.3.2, compliment each other to produce this result. The presence of organic components in the sea lowers the surface tension and renders the production of more and smaller bubbles. Even more important for the predominance of small size bubbles in sea is the inhibition of the process of coalescence by the organic layer on their walls. Finally, the organic skin stabilizes the small bubbles against mass diffusion so that the loss of small bubbles by dissolving is diminished.

3.6.5 Recent measurements

The most recent measurements on bubbles generally follow the parameterization outlined above. The bubble size distributions obtained by de Leeuw and Cohen (1995) in North Atlantic, Geißler and Jähne (1995) in the wind wave facility of Delft Hydraulics, and Loewen et al. (1995) in laboratory with mechanically generated waves are reproduced in Figure 3.3. These results are normalized with the total bubble counts, as described above (Wu, 1988a), to provide the frequency of occurrence p(d) and are compared with the theoretical expression in Figure 3.4a. The wind dependence of the total bubble population for de Leeuw and Cohen (1995) and Geißler and Jähne (1995) data is plotted in 3.4b. The results obtained by de Leeuw and Cohen show no distinct wind dependence. For this particular experiment they encountered the problem of distinguishing bubbles from other particle by their instrumentation. Most probably the counting of additional objects masked the wind influence.

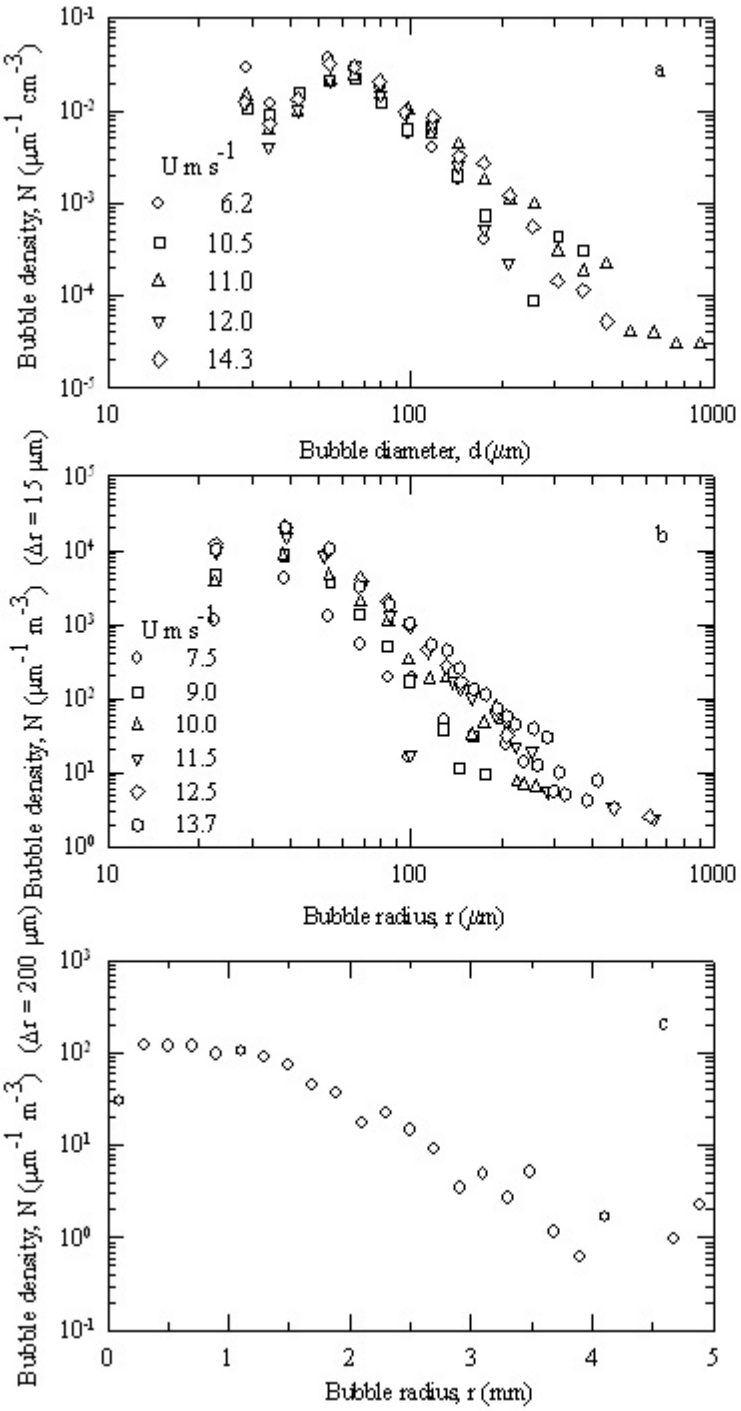

Fig. 3.3 Bubble density as a function of bubble size (radius or diameter) obtained by: a) de Leeuw and Cohen (1995); b) Geißler and Jähne (1995); c) Loewen et al. (1995).

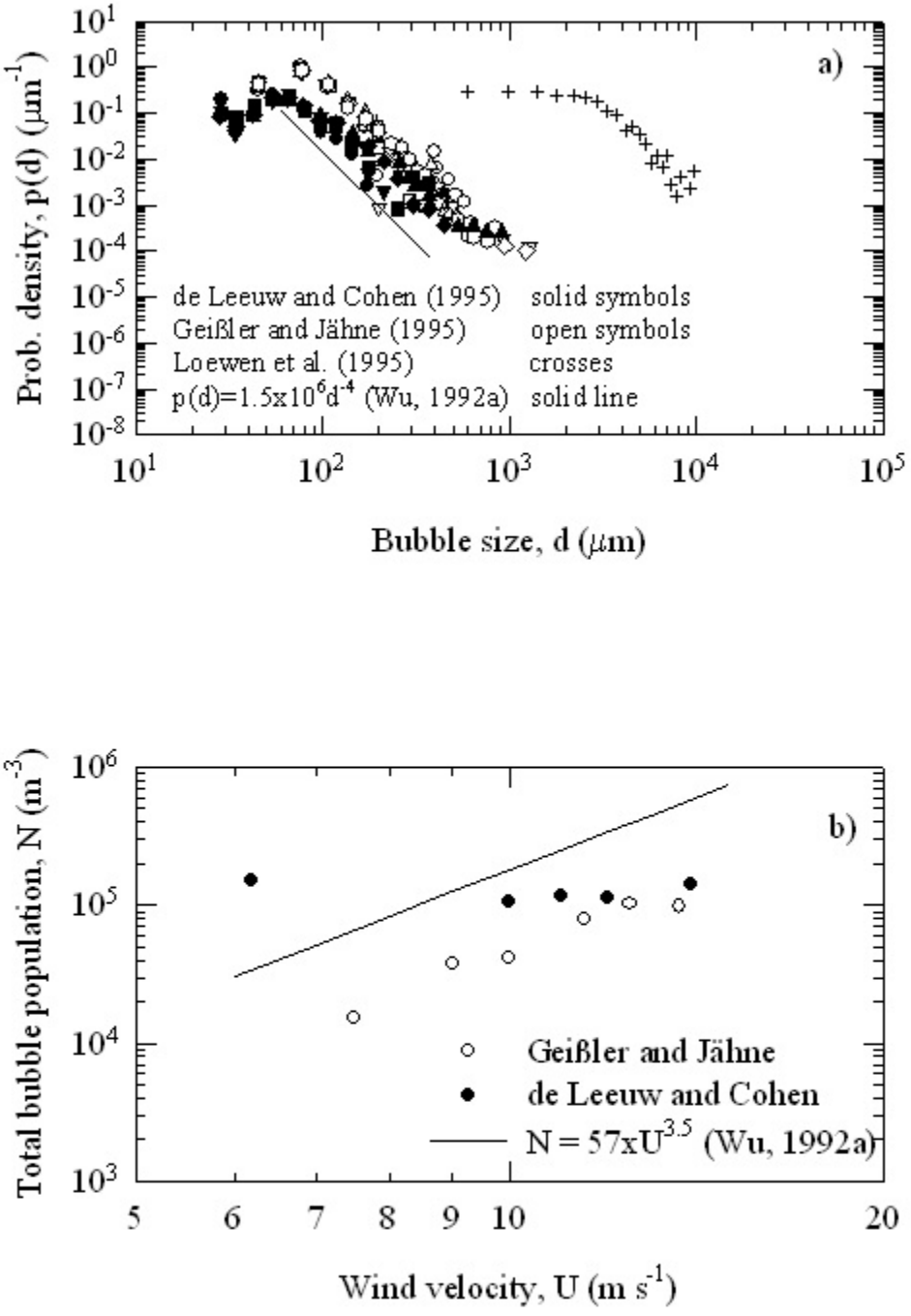

Fig. 3.4 a) Bubble size distributions at various wind velocities: the results were obtained by de Leeuw and Cohen, Geißler and Jähne, and Loewen et al b) Wind dependence of the total number of bubbles: the results were obtained by de Leeuw and Cohen, and Geißler and Jähne.

3.7 Previous Studies on Bubble Clouds

3.7.1 Field Measurements

Thorpe (1982) observed clouds of small bubbles with an upward-pointed sonar at two sites - respectively fresh (Loch Ness) and sea waters (sea near Oban) . The acoustic scattering cross section per unit volume, M_v, of bubbles was measured at several depths. This acoustically derived quantity is a measure for the bubble density. It was found that at constant depth M_v distributions are close to logarithmic normal. These results together with their wind dependancy, reproduced by Wu (1988a), are shown in Figure 3.5. The time-averaged value of M_v decreases exponentially with depth. This value at the same depth and at the same wind speed are greater in the sea than in the fresh-water. The depth penetration in fresh water was found to be of order of half the mixing layer depth. Two distinct types of bubble clouds are discerned: "columnar clouds" which appear in unstable or convective conditions when the air temperature is less than the surface water temperature, and "billow clouds" which appear in stable conditions when the air temperature exceeds that of the water. Clouds penetrate deeper as the wind speed increases, and deeper in convective conditions than in stable conditions at the same wind speed. Gas flux is small at winds up to 12 m s^{-1}, especially for fresh water, but is significant at sea. At higher wind speeds the bubble contribution dominates in the processes of air-water gas transfer.

Walsh and Mulhearn (1987) used a photographic technique to measure bubble size spectra at depths of 0.5 - 2 m under wind speeds of 2 - 14 m s^{-1}. They calculated the void fraction from these spectra. Bubble size spectra at depth 0.5 - 0.6 m and different wind

Figure 3.5 Variations of acoustic scattering cross sections with a) depth, and b) wind velocity at 1-m depth (from Wu (1988a) .

velocities are replotted in Figure 3.6a. In the figure concentrations from 10^3 to 10^4 m^{-3} over radius range of 50 - 300 μm are seen. The probability density of occurrence, obtained by normalizing these spectra with the total number of bubbles, varies with the radius as r^{-4} (the line in Figure 3.6b) . The number of larger bubbles increased with increasing the wind speed, and at 10 - 14 m s^{-1} bubbles larger than 200 μm occurred at all depths whilst at low winds (6 - 9 m s^{-1}) no bubbles greater than 200 μm were counted. The authors observed bubble population to be highly variable with time, with large deviations from the mean

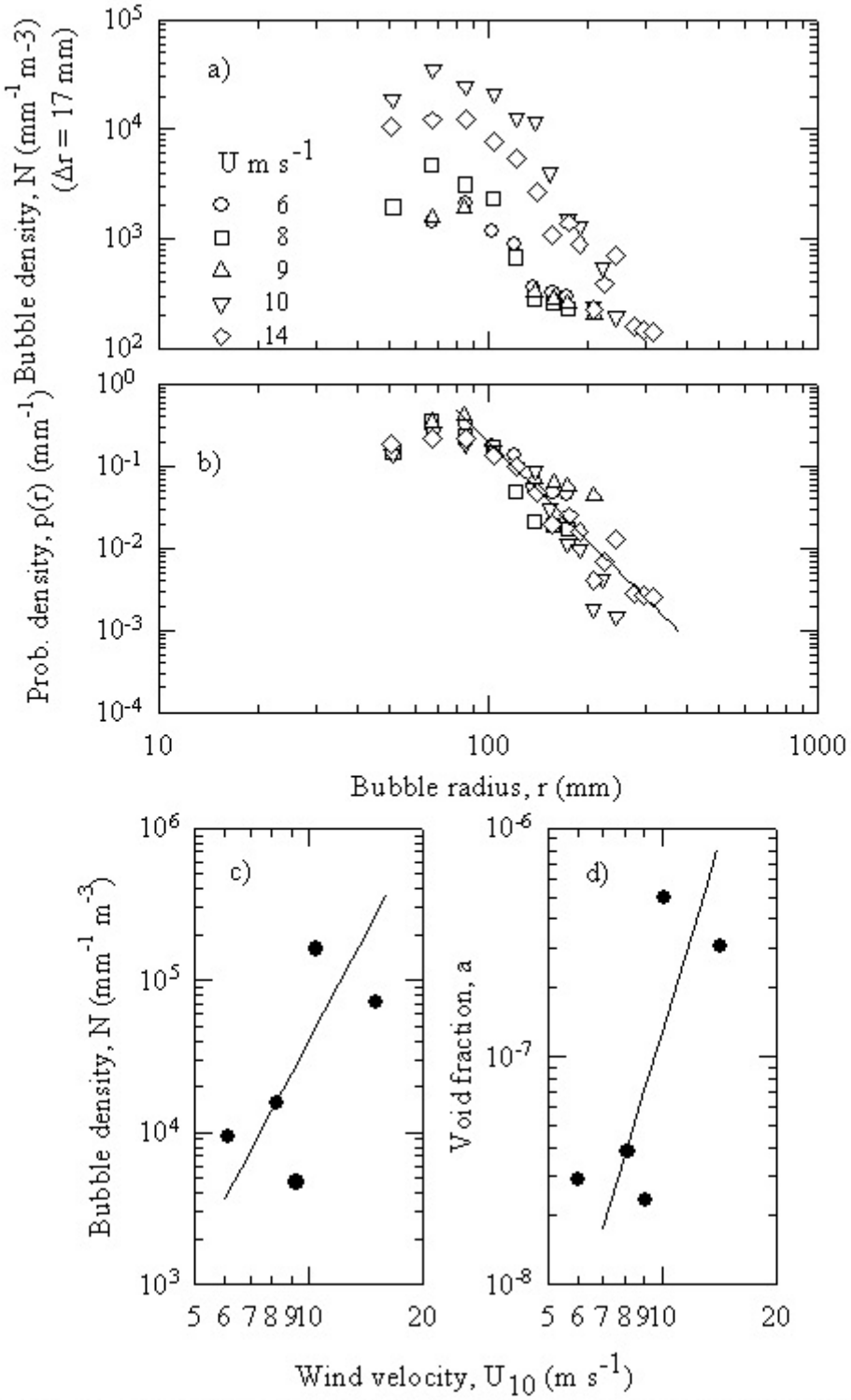

Fig. 3.6 Results obtained by Walsh and Mulhearn (1987): a) Bubble size spectra at depth 0.5 - 0.6 m and various wind velocities; b) Probabilty density varies as r^{-4}; Wind dependence of c) bubble density and d) void fraction.

bubble density, and attributed it to the generation of bubble clouds from the breaking near the camera. They reported the bubble density at all depths (0.5 - 2 m) to vary as $U^{3.3}$, air volume fraction followed $U^{4.9}$. Accounting for the depth dependency of the bubble spectra, Wu (1992b) separated the results for different depths and found wind dependency $U^{4.7}$ and $U^{5.5}$ for bubble density and air volume fraction, respectively. The plots for both quantities at depth 0.5 - 0.6 m are shown in Figure 3.6c and 3.6d.

Melville et al. (1995) more recently used an acoustic technique to measure the void fraction and bubble size distribution in The North Atlantic. A merit of their work is the continuous monitoring during 1993-1994 winter. The data for low-frequency sound speed was inverted to give the volume fraction of air in the sampling volume while the inversion of broad-band sound speed and attenuation data provided measurements of bubble size distribution. They believe they can resolve air fractions in a cubic meter of water as small as $O(10^{-7})$. The depth, z, dependence of a void fraction can be well fitted with exponential law or power law, z^{-3} (Figure 3.7a) . Time variation of void fraction α for two days is given in Figure 3.7b. Void fractions in the range 10^{-4} - 10^{-6} m^{-3} are registered. It worth noting in this figure that the values of the void fraction at depth 0.7 m (circles) and those over the whole depth from 0.7 to 7 m (squares) differ only slightly. Hence, the void fraction values measured at the surface are enough representative for the entire water column. From acoustic data, solving an integral equation, they inferred the number of bubbles in the sampling volume and over a range of radii (60 - 400 μm) . Bubble density is in order of 10^9 for the small bubbles and 10^6 for larger bubbles. The inverse problem can be resolved using

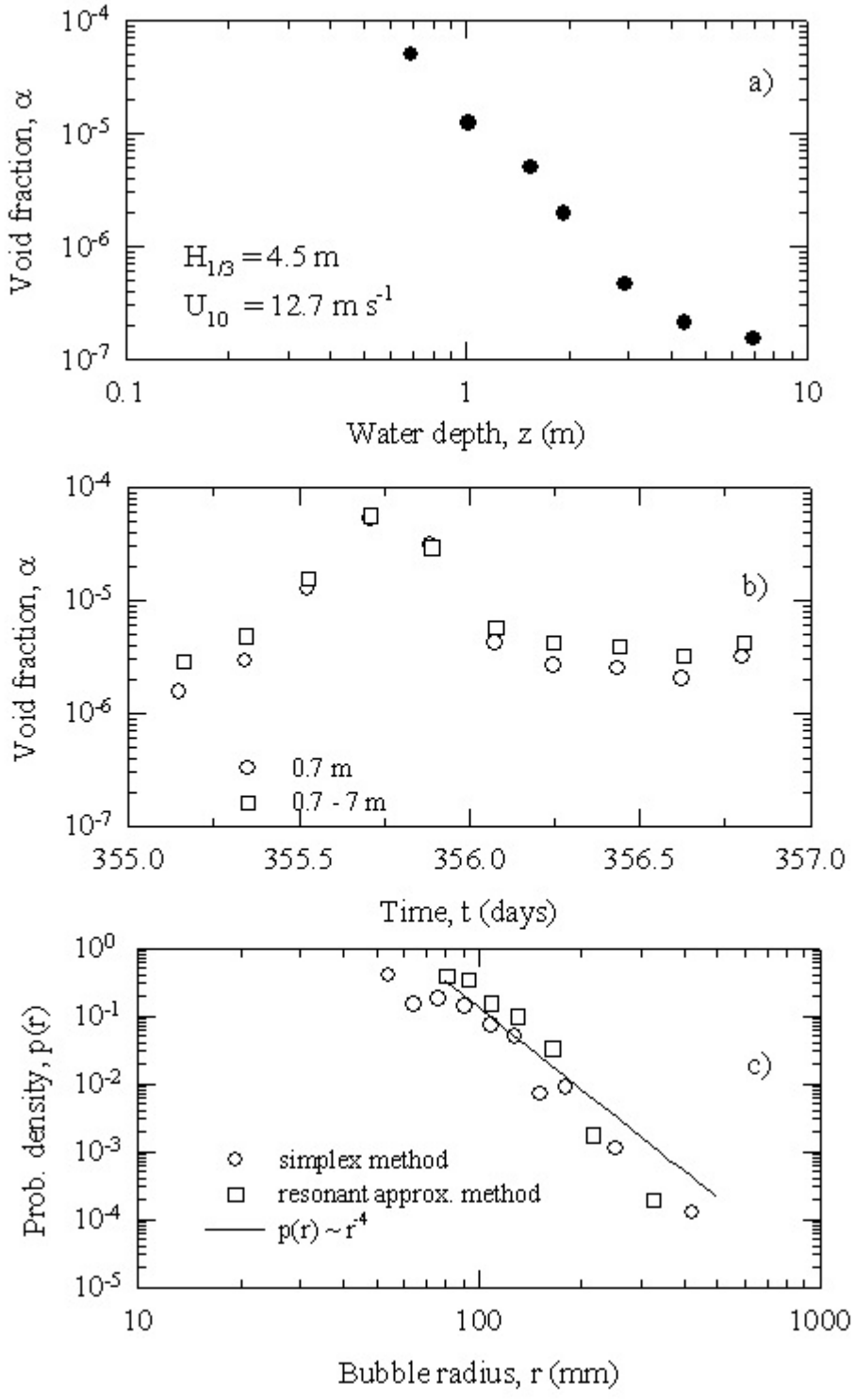

Fig. 3.7 Results obtained by Melville et al. (1995): a) Depth dependency of the void fraction
b) void fraction at depth 0.7 m and for water column 0.7 - 7 m;
c) Bubble size spectra from acoustic data obtained with two methods.

two methods. The first method, a simplex method, is based on the assumption that main contribution to sound backscattering or attenuation is from bubbles with a resonance frequency near the frequency of the sounding impulse. The second method, a resonant approximation method, is based on the finding that off-resonance contributions are also important, i.e., the contributions due to all bubble sizes are included. Probability densities of occurrence, result of normalizing the bubble distributions obtained with the two methods, generally follow r^{-4} law (Figure 3.7c) .

Dahl and Jessup (1995) carried out an experiment to measure the time-varying properties of bubble clouds as they evolve from ocean breaking waves. The experiment was conducted from the floating instrument platform *Flip* and consisted of simultaneous, colocated acoustic measurements of subsurface bubbles and video recording of the sea surface. Only two wave-breaking events were amenable to detailed analysis, and the authors did not characterize the stochastic variability. From the video records the phase speed of the breakers was estimated and then characteristics length λ_c and time T_c were derived from the dispersion relation. These were used to scale the spatial and temporal characteristics of the clouds. The entrainment depth of the bubbles is presented for times after $3T_c$, as the acoustic device is sensitive to the longer time scale evolution. The measured depth of penetration was corrected for bubble rise speed and scaled favorably with the characteristics length and time. They propose an empirical fit to their results describing the evolution of the bubble cloud with the depth: $D/\lambda_c \propto (t/T_c)^{0.7}$. The void fraction was calculated from the acoustic backscattering cross section; values of order 10^{-8} were obtained for depth about 1.5 m.

3.7.2 Laboratory Measurements

Lamarre and Melville (1991) reported measurements of air entrainment by controlled deep-water breaking waves with a void-fraction gauge. They registered void fractions over the full (0-100%) range, and voids > 20% for the sampling volume (channel width b times the cross-sectional area of the bubble plume) were sustained for up to half a wave period after breaking. The parameters they discussed included the total volume of entrained air V, cross-sectional area of the bubble plume A, mean void fraction α, potential energy of the bubble plume E_b, and horizontal, x, and vertical, z, centroids of the void-fraction. These quantities (normalized accordingly with the maximum volume measured V_o, the total energy dissipated by breaking E_d, and the wave length λ) versus time (normalized with the time of initial motion of the wavemaker t_b and wave period T) are shown in Figure 3.8. They estimated that the mean void fractions in the sampling volume remain above 1% within the first wave period after breaking (Figure 3.8c) . The horizontal centroid moves at roughly the phase speed of the wave for half period (Figure 3.8e); the vertical centroid below the undulating surface is almost constant (Figure 3.8f) . Preliminary experiments for void-fraction gauge performance were accompanied with still photographs, (Figure 3.9); the formation and evolution of distinct bubble plumes were qualitatively compared (Lamarre, 1993) .

Kalvoda (1992) parameterized clouds of large bubbles produced by breaking wind waves at wind velocity of 16 m s^{-1} in a laboratory tank using a photographic approach. From side and top views the temporal evolution of these macrobubble clouds, including their

Figure 3.8 Results obtained by Lamarre and Melville (1991) . For details see the text.

length scales, aspect ratio, area scale, and velocity, is provided. Bubble concentration and void fraction within the cloud are also reported. The initial horizontal velocity of the cloud is estimated to be from one half to two thirds the phase velocity of breaking wave. The main conclusions of this work are: the bubble cloud grows in depth (side view) and in width (top view) differently; the maximum penetration depth approaches one half the wave height; the maximum cloud lengths at the top and side views are 0.1 and 0.16 of the wave length, respectively; the average horizontal cloud speed is about 0.45 times phase speed; the void fraction is about 0.4% for air-water volume estimated as the product of side-view area and

the top-view width of the cloud; the concentration of microbubbles within the cloud varies with diameter as $d^{-3.2}$ for diameter range 1 - 10 mm.

Figure 3.9 Comparison of the bubble plume registered with a void-fraction gauge and photographic technique (from Lamarre, 1993) .

3.7.3 Discussion

The field (Thorpe, 1982) and laboratory (Kalvoda, 1992) experiments on measurements and observation of the time evolution of the bubble cloud shape show clearly that this approach is useful in gaining insights for the dynamics of the mixing processes. The scaling of bubble cloud dimensions with the wave characteristics (Kalvoda, 1992) is appropriate for connecting the laboratory and field data.

The values of void fraction reported for both field and laboratory measurements are in the range 10^{-8} - 10^{-1}. There are reasonable explanations for the wide discrepancies among the void fraction values from different investigators. Lamarre and Melville (1991) report void fraction values > 1% up to 100% beneath plunging breakers very close to the surface, at depths 0.05 m and 0.15 m. Kalvoda (1992) calculates void fraction values of 0.4% from bubble size distributions under spilling breakers and neglecting bubbles residing very near to the surface. In addition, the volumes of the air-water mixture, from which the void fractions are calculated, in the two studies are different; 90 cm^3 for the former and 700 - 1000 cm^3 for the latter. Also, Kalvoda (1992) counts only relatively large bubbles (2 - 10 mm in diameter), while Lamarre and Melville (1991) result includes probably wider diameter range and more small bubbles. Lastly, the lower threshold of the void fraction gauge is 0.3% (Lamarre, 1993) and it is insensitive to very low void fraction values. Meanwhile, Walsh and Mulhearn (1987) values of void fraction, also calculated from bubble size population as Kalvoda (1992), are in the range 10^{-6} - 10^{-7} m^{-3} in ocean. Compared with Kalvoda's result (1992) these value though lower, seem to be reasonable as the depth of

measurements is 0.6 m and the strongest wind is 14 m s^{-1} (Kalvoda (1992) measurements are at 16 m s^{-1} wind) . Walsh and Mulhearn (1987) values are also lower than the Melville et al. (1995) values (10^{-4} - 10^{-6} m^{-3}) taken slightly deeper (0.7 m) but in winter conditions characterized with stronger winds (up to 18 m s^{-1}) . Though explainable, the differences in void fraction values hamper the comparison and analysis of data, and ultimately the conclusions based on them. It is known, and seen from the numbers above, that the void fraction is a spatially averaged variable whose value depends on the size of the measuring volume (Melville et al., 1993) . It is important, therefore, this volume to be always carefully determined and reported.

It is also of great interest to find a way to estimate the bubble population from the void fraction measured, i.e., to solve the inverse problem. For acoustically measured void fraction values this task is solved using an integral equation (Melville et al., 1995; Lamarre, 1993) . This thesis presents an alternative way to solve the inverse problem for void fraction values measured by utilizing imaging technique, and the results are encouraging.